Study of Ice Crystal Orientation in Cirrus Clouds Based on Satellite Polarized Radiance Measurements

VINCENT NOEL

Analytical Services and Materials, Hampton, Virginia

HÉLÈNE CHEPFER

Laboratoire de Météorologie Dynamique, Ecole Polytechnique, Palaiseau, France

(Manuscript received 8 May 2003, in final form 3 February 2004)

ABSTRACT

The goal of this paper is to retrieve information about ice particle orientation in cirrus clouds. This is achieved by comparing simulations of sunlight reflection on a cirrus cloud with measurements of polarized radiances from the spaceborne instrument Polarization and Directionality of the Earth's Reflectance (POLDER-1) on *Advanced Earth Observing Satellite-1* (*ADEOS-1*). Results show that horizontal orientation of crystals can be spotted by the presence of a local maximum of polarized radiance in the direction of specular reflection. The angular width of the local maximum is shown to contain information on the particle maximum deviation angle, while the maximum intensity can provide information on particle shape and relative concentrations of ice crystals, horizontally and randomly oriented. The study of 31 ice cloud cases show that in 80% of them, the deviation angle is less than 3°. Also, the relative concentration of horizontally oriented crystals is less than 21%, depending on the angular distribution used for crystal deviation.

1. Introduction

Cirrus clouds cover permanently more than 30% of the earth's surface (Wylie et al. 1994), and as such have a strong influence on the planet's radiative balance (Stephens et al. 1990). As they are made of ice crystals, their influence strongly depends on their microphysical properties. However, for cirrus clouds such properties show a very high variability, and due to the high altitude of these clouds in situ data is only scarcely available. As a consequence, the overall cirrus radiative impact is still uncertain, with one of the largest sources of uncertainty remaining the microphysical properties, and especially the particles' orientation in space.

Usually, studies of crystal properties inside cirrus clouds implicitly assume a random orientation for the particles. This type of model has symmetry properties that allow great simplification in computations of crystal optical properties and radiative transfer. Nowadays, this model is still used in the vast majority of radiative transfer simulations used to parameterize cirrus clouds models. However, it cannot give a satisfactory explanation for all optical displays created by these clouds, and could lead to possible bias when estimating their radiative impact.

First observations of preferential orientation of ice crystals were done through stroboscopic measurements (Magono 1953), refined several years later by studying droplets' accretion on falling ice particles (Ono 1969). These first studies revealed that specific shapes of ice crystals, such as plates, columns, and dendrites, oriented themselves while falling, in order to offer maximum resistance to the air. As in situ observation of this dynamic behavior is not possible, remote sensing was gradually introduced in the studies that followed. Radar (Hendry and McCormick 1976) and direct photography (Sassen 1980) were used first; however, the instrument that generated the most studies of the orientation phenomenon is the lidar (Platt et al. 1978; Sassen 1980; Thomas et al. 1990; Sassen and Takano 2000; Noel et al. 2002), thanks to its ability to detect optically thin clouds and its sensitivity to light polarization.

Theoretical and laboratory studies (Jayaweera and Mason 1965; Podzimek 1968; List and Schemenauer 1971; Lynch et al. 1994; Klett 1995) gave further insight into this behavior. Computer simulations (Takano and Liou 1989a) showed that oriented crystals could increase the cloud albedo by as much as 30%, leading to important modifications on the cloud–radiative effect (Takano and Liou 1989b). Recent observations (Sassen et al. 2003) suggest crystal orientation could even have

Corresponding author address: Vincent Noel, NASA Langley Research Center, Mail Stop 435, Hampton, VA 23681-2199.
E-mail: v.r.noel@larc.nasa.gov

a potential feedback effect on particle generation inside the cloud. These results confirm the possible impact of this parameter on climate prediction. Unfortunately, the frequency and concentration of horizontally oriented crystals at a global scale in ice clouds is still largely unknown.

In order to estimate the overall impact of crystal orientation on cloud radiative effects, studies have to be pursued on a global scale, which is only possible through satellite monitoring. Following this approach, radiance observations from satellite instruments have been found to convey information about cirrus cloud microphysical properties (Chepfer et al. 2001, 2002; Liou and Takano 2002; Masuda et al. 2002). More specifically, Polarization and Directionality of the Earth's Reflectance (POLDER-1) observations of sunlight scattering upon ice clouds were recently used to estimate the frequency of the preferred orientation of crystals in cirrus clouds (Chepfer et al. 1999). The present paper focuses on the cases where oriented crystals were actually observed. Measurements of normalized polarized radiances are compared to results of ray-tracing simulations to retrieve informations about crystal orientation behavior.

The observations and the simulations are presented in section 2, followed by the sensivity study of simulated normalized polarized radiances to crystal microphysical properties (section 3). Based on these findings, the horizontally oriented crystal maximum deviation angle and relative concentrations are retrieved in section 4. Discussion and conclusions are given in section 5.

2. Observed and simulated radiances

a. Observed radiances from satellite

The preferential orientation of ice crystals in a cirrus cloud creates physical anisotropy that can be detected with multidirectional observations. For example, in the presence of horizontally oriented plates, bidirectional polarized radiances show a distinctive high-intensity peak in the direction of specular reflection. This distinctive behavior has been used to estimate the frequency of horizontal orientation of crystals in cirrus clouds (Chepfer et al. 1999), using observations of normalized polarized radiances reflected by the atmosphere from the POLDER-1 spaceborne radiometer.

POLDER-1 (Deschamps et al. 1994) flew on the *Advanced Earth Observing Satellite-1* (*ADEOS-1*) satellite from August 1996 to June 1997 and, up to now, seems the best-suited instrument to retrieve information about crystal orientation in cirrus clouds. This radiometer measured normalized radiances $L_n(\theta_v, \varphi_v)$ and normalized polarized radiances $L_{n,p}(\theta_v, \varphi_v)$ for a given ground or cloud pixel from up to 14 viewing directions, defined by their zenith and azimuthal angles θ_v and φ_v (Hagolle et al. 1999):

$$L_n(\theta_v, \varphi_v) = \frac{\pi L(\theta_v, \varphi_v)}{\cos\theta_s E_s} \qquad L_{n,p}(\theta_v, \varphi_v) = \frac{\pi L_p(\theta_v, \varphi_v)}{\cos\theta_s E_s} \tag{1}$$

with θ_s the solar zenith angle and E_s the solar irradiance at the top of the atmosphere. The quantities $L_n(\theta_v, \varphi_v)$ and $L_{n,p}(\theta_v, \varphi_v)$ were measured at several visible wavelengths (443–865 nm). In order to minimize bias due to molecular scattering, this study uses the 865-nm channel.

To simulate $L_n(\theta_v, \varphi_v)$ and $L_{n,p}(\theta_v, \varphi_v)$, multiple-scattering effects have to be considered (section 2b).

b. Normalized polarized radiance and multiple scattering

Multiple scattering has been shown to have a significant impact on light scattered by randomly oriented particles (Trankle and Greenler 1987). However, in presence of horizontally oriented particles, its impact on normalized radiances is still not correctly quantified, even if its influence on plane albedo has been estimated (Takano and Liou 1989b). In such a case, a reasonable guess would be to assume this impact is similar in preferential and random orientation. For this last case, studies of multiple-scattering effects on total and polarized radiances (Goloub et al. 1994) have shown that, while the total radiance is strongly affected by multiple scattering, polarized radiance is mainly formed by the first scattering event, with saturation quickly taking place after a few events and no further influence from following events. Hence, if an observed cloud has an optical depth high enough for the polarized radiance to reach saturation, the reflected normalized polarized radiance no longer depends on the cloud optical depth.

In such cases, it is possible to write a single-scattering approximation of normalized polarized radiance from the general radiative transfer equation (Goloub et al. 1994):

$$L_{n,p}(\theta_v, \varphi_v) = \frac{\cos\theta_s}{4(\cos\theta_s + \cos\theta_v)}\sqrt{Q^2 + U^2 + V^2} \tag{2}$$

with Q, U, and V the second, third, and fourth elements of the scattered Stokes vector (Van de Hulst 1957). This approximation has already been widely used in the litterature (C. Labonnote et al. 2000, 2001; Goloub et al. 2001; Riedi et al. 2000, 2001). In order to ensure its validity, all the cases selected for the present paper (section 4) have a high optical depth.

c. Simulated radiances from modeled crystals

Following Eq. (2) the scattered Stokes vectors are sufficient to simulate normalized polarized radiances $L_{n,p}(\theta_v, \varphi_v)$ for any viewing direction in space. The Stokes vectors were simulated using a ray-tracing code (Noel et al. 2001), for clouds composed of preferentially oriented crystals.

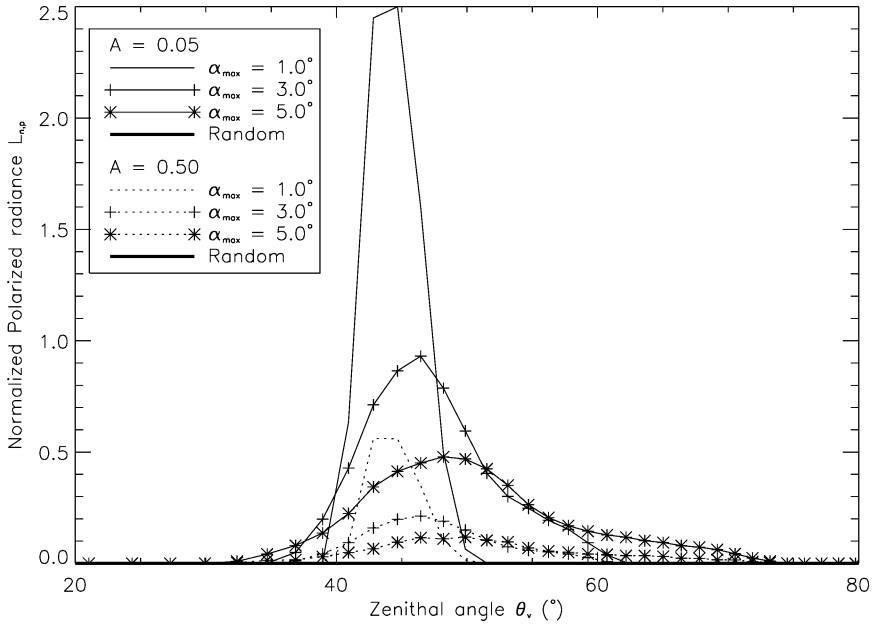

FIG. 1. Normalized polarized radiance as a function of zenith angle θ_v.

As a first approximation, the modeled ice crystals were shaped as hexagonal-based plates with variable aspect ratios $A = l/2r$ (with l the crystal length and r the radius of the hexagonal base). This simple shape seems to accurately reproduce the scattering behavior of cirrus clouds (Heymsfield and Platt 1984). The plates are also the particles more likely to exhibit a preferential orientation with a specific optical signature (Ono 1969; Sassen and Takano 2000). Preferential orientation is taken into account in the model through the deviation angle α from the horizontal plane. As the general distribution of α is still unknown, both Gaussian and square probability functions are considered, both centered on $\alpha = 0°$, with a standard deviation $\alpha_{\max}$. In this framework, $\alpha_{\max}$ gives an indication of the average deviation of ice crystals from the horizontal plane, with $\alpha_{\max} = 0°$ meaning a perfect horizontal orientation.

Once the crystals' parameters A and $\alpha_{\max}$ are chosen, and the solar zenith angle θ_s is fixed, the ray-tracing simulation delivers the entire 4×4 scattering matrix $\mathbf{M}(\theta_v, \varphi_v)$ of the modeled crystal for any viewing direction in space. As incident sunlight is unpolarized [i.e., its Stokes vector is $\mathbf{I} = (1, 0, 0, 0)$], the Stokes vector of the scattered light (Van de Hulst 1957) is easily obtained by

$$\mathbf{I}_s(\theta_v, \varphi_v) = M(\theta_v, \varphi_v)(1, 0, 0, 0) = \sum_{i=1}^{4} M_{i,1}(\theta_v, \varphi_v). \quad (3)$$

Normalized polarized radiances are then easily calculated using Eq. (2).

3. Study of simulated polarized radiances

a. Sensitivity study

For the sake of simplicity, in this sensitivity study scattering is considered in the primary scattering plane ($\varphi_v = \varphi_s = 0$), with a solar incidence angle arbitrarily fixed at $\theta_s = 43°$. For actual case studies (section 4) the exact scattering plane and incidence angle measured by POLDER-1 will be used.

As an example, the simulated normalized polarized radiance $L_{n,p}$ reflected by the cloud is plotted in Fig. 1 as a function of the zenith angle θ_v, for three square distributions of deviation angles with $\alpha_{\max} = 1°, 3°, 5°$, and two crystal aspect ratios $A = 0.05$ and 0.5. The comparatively low $L_{n,p}$ for randomly oriented crystals is plotted in the bold line. In these curves, $L_{n,p}$ shows a local maximum in the direction of specular reflection ($\theta_v = 43°$), which is not present for randomly oriented particles.

Similar computations using a Gaussian distribution for the deviation angle α give a similar shape for $L_{n,p}$ and have not been plotted in Fig. 1 for readability. However, properties of the simulated curves depend strongly on the chosen distribution (square or Gaussian) and on the value of $\alpha_{\max}$. Similarly, the particle aspect ratio has a strong influence.

1) SENSITIVITY TO CRYSTAL MAXIMUM DEVIATION ANGLE

The general shape of the curve is strongly dependent on the crystal maximum deviation angle $\alpha_{\max}$ (Fig. 1). For crystals with small deviation angles, the curve

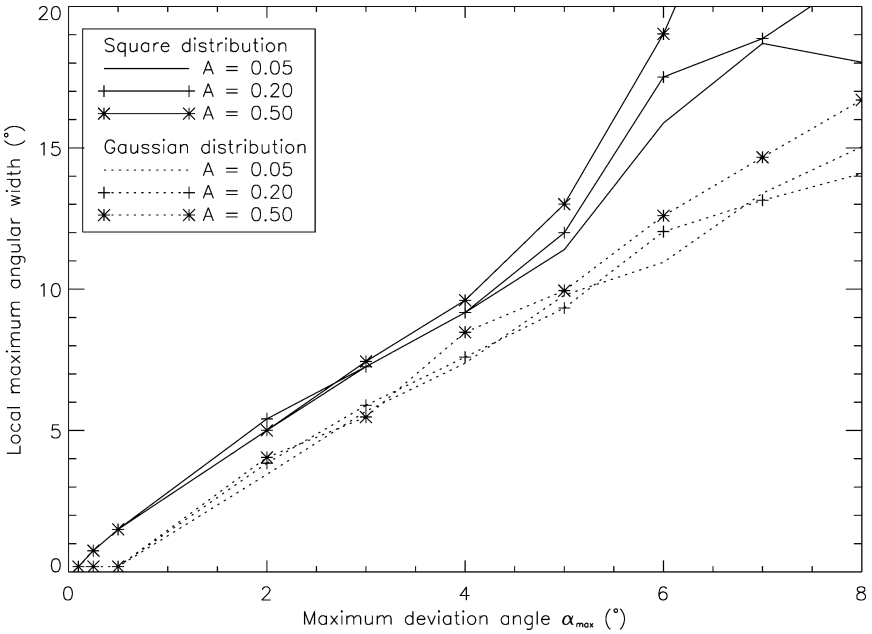

FIG. 2. Local maximum angular width as a function of maximum deviation angle α_{max}.

shows a very narrow peak of high intensity in the direction of specular reflection. If the crystal deviation angle increases, the maximum intensity quickly decreases, while its angular width increases. This behavior reaches its limit for randomly oriented crystals: the local maximum totally disappears.

The peak angular width, at half-maximum intensity, is plotted in Fig. 2 as a function of the crystal maximum deviation angle α_{max} for three different aspect ratios: 0.05, 0.2, and 0.5. For square distributions of the deviation angle α, very small deviations ($\alpha_{max} \simeq 1°$) show a local maximum with a 2° angular width. This width increases very quickly with crystal deviation, gaining approximately 5° for a 2° increase in α_{max}. For Gaussian distributions the angular widths are smaller (i.e., the peaks are narrower) by 1.5° in average, due to the higher probability given to smaller angular deviations. If the deviations are too small (i.e., $\alpha_{max} < 0.5°$), the angular width becomes too narrow to be measured. With both distributions, the curve is monotonic for small deviation angles ($\alpha_{max} < 6°$, angular width up to $\simeq$15°). The maximum deviation angle α_{max} can then be linked to the angular width of the local maximum, independently from the aspect ratio.

The curve maximum intensity is plotted in Fig. 3 as a function of crystal aspect ratio A for three maximum deviation angles α_{max}: 1°, 2°, and 3°. The maximum intensity is very sensitive to the crystal deviation angle small deviations lead to high intensities, and a 1° increase in α_{max} leads to a 50% fall in maximum intensity. In addition, the effect of crystal aspect ratio A is more apparent on the maximum intensity (Fig. 3) than on the peak angular width (Fig. 2).

2) SENSITIVITY TO CRYSTAL SHAPE

The crystal aspect ratio A has a more subtle impact on the polarized radiance. For small crystal deviation angles (α_{max} up to 6°), the aspect ratio has almost no influence on the curve angular width (Fig. 2). When deviations get larger ($\alpha_{max} > 6°$), the crystal aspect ratio begins to influence the curve angular width. This is equally valid without regard to the distribution chosen for α.

The influence of crystal shape is more obvious when looking at the curve maximum intensity. For square distributions, low aspect ratios ($A < 0.15$) lead to high normalized polarized radiances $L_{n,p} > 8$ (Fig. 3). When the aspect ratio increases, the polarized radiances decreases, with a threshold for $0.2 < A < 0.3$ due to consecutive scattering events inside the crystal. There can be a factor of 10 between local maximum intensities for very low ($A < 0.05$) and very high ($A \simeq 1$) aspect ratios. For a Gaussian distribution, the same behavior is observed; however, the maximum intensities are significantly increased, up to 400% for $\alpha_{max} = 1°$. This will have important consequences on the retrieved microphysical properties (section 3b).

3) SENSITIVITY TO CRYSTAL CONCENTRATIONS

Until this point of the study, clouds were assumed to be only composed of horizontally oriented crystals. However, it is possible that only a fraction of crystals are closely aligned with the horizontal plane, while the remaining crystals are randomly oriented. If a cloud is defined as a mix of horizontally oriented crystals (noted

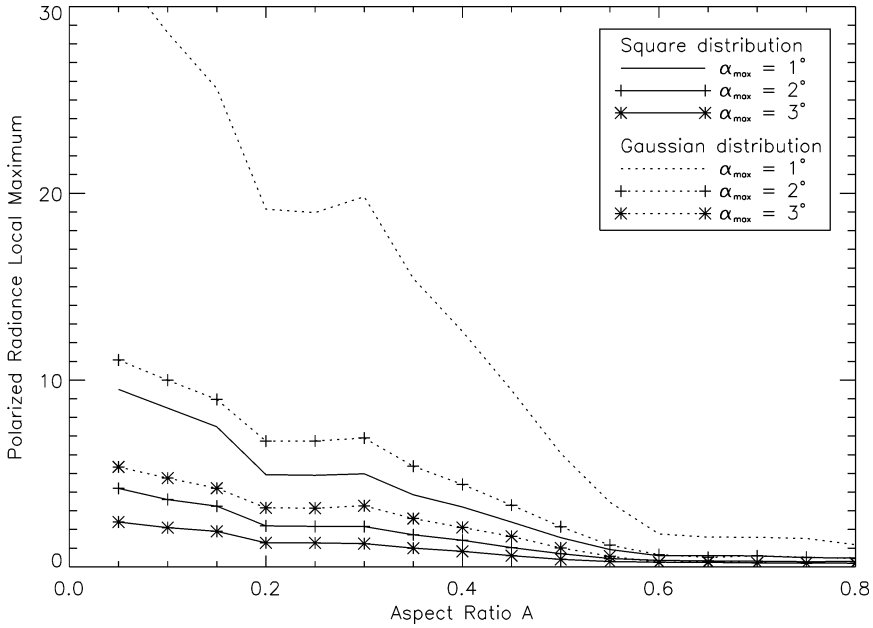

FIG. 3. Maximum normalized polarized radiance intensity as a function of crystal aspect ratio *A*.

by the subscript *h*) and randomly oriented crystals (noted by the subscript *r*), the normalized polarized radiance $L_{n,p}$ scattered by the entire cloud will be given by (Sassen and Benson 2001):

$$L_{n,p} = \frac{n_h L_{n,p,h} + n_r L_{n,p,r}}{n_h + n_r}, \tag{4}$$

where n is the relative concentration of each particle bearing the relevant orientation, and $L_{n,p}$ the related radiance [Eq. (2)]. For randomly oriented crystals there is no normalized polarized radiance maximum in the direction of specular reflection, thus $L_{n,p,r} \ll L_{n,p,h}$ (typically, for a solar zenith angle $\theta_s = 43°$, $L_{n,p,r} < 0.014$ in the direction of specular reflection). If $L_{n,p,r}$ is neglected, the total normalized polarized radiance is given by $L_{n,p} = [n_h/(n_h + n_r)]L_{n,p,h}$. The local maximum of normalized polarized radiance will linearly decrease as the quantity of randomly oriented particles increase.

b. Retrieval of cloud microphysical properties

Following the sensivity study (section 3a), microphysical properties of the studied cloud can be retrieved using observed normalized polarized radiances.

In a first step, the crystal maximum deviation angle $\alpha_{\max}$ can be retrieved from the angular width of the polarized radiance local maximum [section 3a(1)], provided the deviations are less than 6° wide. As Gaussian distributions lead to slightly thinner peaks for a given $\alpha_{\max}$ (Fig. 2), stronger deviations will be required to produce a given angular width.

Once $\alpha_{\max}$ is known, the intensity of the polarized radiance local maximum can be estimated as a function of crystal aspect ratio *A* and relative concentration of horizontally oriented particles n_h [sections 3a(2) and 3a(3)]. Gaussian distribution leads to higher intensities (Fig. 3), so lower concentrations will be required to produce a given intensity. These two values are correlated, and sets of possible values can be retrieved based on the actual polarized radiance measurements.

As an example, the maximum intensity of $L_{n,p}$ is shown in Fig. 4 as a function of crystal aspect ratio *A*

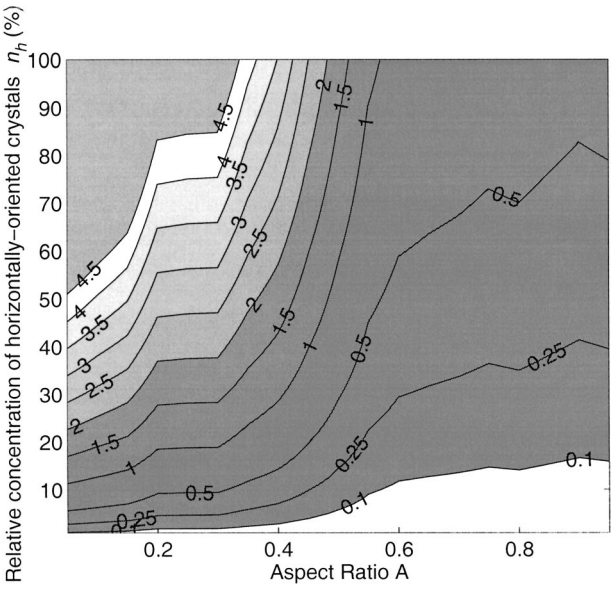

FIG. 4. Normalized polarized radiance local maximum (0.1–4.5, contour interval 0.5 above 0.5) as a function of crystal aspect ratio *A* and horizontally oriented crystals' relative concentration n_h.

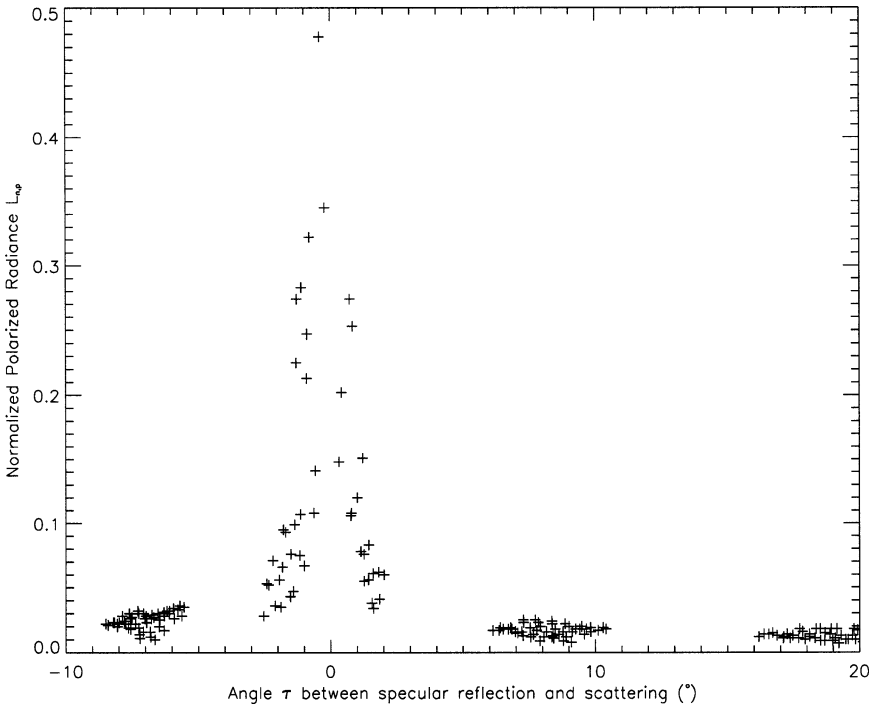

FIG. 5. Normalized polarized radiance as a function of the angle τ between the specular and scattering directions.

and horizontally oriented crystal relative concentration n_h, for a square distribution of deviation angles with $\alpha_{\max} = 1°$. Using this figure, an observed polarized radiance maximum intensity can be linked to a range of correlated values for A and n_h. In this specific case, cloud areas showing polarized radiance values greater than 3 should contain more than 30% of horizontally oriented crystals, the exact value depending on their shape.

4. Studied case

a. Case study

Each case must be studied for the actual viewing angles θ_v, φ_v, for which the azimuth angle $\varphi_v - \varphi_s$ is rarely constant. Therefore, polarized radiances are considered as a function of the angle τ between the direction of specular reflection and the actual scattering direction. The local maximum of polarized radiance is therefore centered on $\tau = 0°$.

The case studied in this section was measured by the POLDER-1 radiometer at coordinates 60.25°N, 25.15°W, through orbit 7352 over the ocean. In this case, sunlight reflected on an ice cloud with incident angle of $\theta_s = 42°$. Measurements of normalized polarized radiance are shown in Fig. 5 as a function of τ. They show a local maximum of $L_{n,p} \simeq 0.5$ in the direction of specular reflection (for $\tau \simeq 0°$), while staying relatively low for other scattering directions. This behavior suggests the presence of horizontally oriented crystals in the studied cloud.

Measurements of polarized radiances are very similar to results from ray tracing simulations (Fig. 1). More specifically, the angular width and intensity of the local maximum lie within the same range. It should then be possible to retrieve the maximum deviation angle and relative concentration of the horizontally oriented crystals present in the cloud, following the steps shown in section 3b.

b. Retrieval of the crystal maximum deviation angle

The angular width of the peak at half maximum intensity is approximately 1.5°. When considering normalized polarized radiance, the angular width of a local maximum is linked to the maximum deviation angle of horizontally oriented crystals in the cloud, with little regard to the quantity or shape of these crystals [section 3a(1)]. To retrieve the maximum deviation angle, simulations are first conducted with an arbitrary large crystal deviation (typically $\alpha_{\max} = 60°$). The simulated normalized polarized radiances are then compared to the actual observations, with respect to the exact scattering direction given by the angles θ_v and φ_v (section 2c). Based on the width difference between the simulated polarized radiances and the measured ones, an adjusted value of the crystal maximum deviation angle is used in a new round of simulations. This whole process is repeated until convergence is reached. The crystal max-

TABLE 1. Relative concentrations of horizontally oriented crystals for different aspect ratios.

Aspect ratio A	0.05	0.1	0.2	0.3	0.4	0.5
Relative concentration n_h (square, %)	0.7	0.8	1.1	1.5	1.7	3.6
Relative concentration n_h (Gaussian, %)	0.5	0.6	0.7	1.0	1.3	3.1

imum deviation angle is the one giving the best agreement between the simulated and measured radiances.

For the actual case, the retrieved crystal maximum deviation is 0.6° considering a square angular distribution and 2.1° considering a Gaussian distribution.

c. Retrieval of horizontally oriented crystals' shape and relative concentration

When considering a local maximum of normalized polarized radiance created by horizontally oriented crystals, its intensity is linked to the shape and relative concentration of these crystals with respect to the angular distribution of the crystal deviation angle [section 3a(3)]. As the crystal maximum deviation angle is obtained independently (section 4b), the shape and relative concentration of these crystals can be retrieved.

The retrieved crystal maximum deviation angles for the actual case are 0.6° and 2.1° (section 4b). Using the retrieved $\alpha_{\max}$ and the exact POLDER-1 observation angle, local maximums of polarized radiances are simulated for different aspect ratios. For each aspect ratio, the relative concentration of horizontally oriented particles n_h is estimated (section 3b). These concentrations are shown in Table 1 for both square and Gaussian angular distributions.

Even if the relative concentration n_h shows high variations for different crystal shapes (the retrieved concentration is between 5 and 6 times higher for $A = 0.5$ than for $A = 0.05$, depending on the deviation distribution), the concentration values stay overall very low, below 4%. As was expected (section 3b), the use of Gaussian distribution leads to lower concentrations.

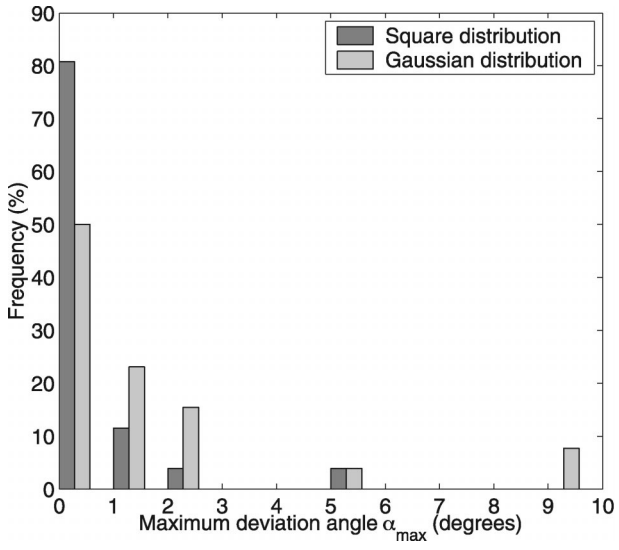

FIG. 6. Frequency of maximum crystal deviation angles $\alpha_{\max}$.

d. Multiple cases

The same analysis is conducted on 30 more cases where POLDER-1 measurements show a local maximum of normalized polarized radiance, and there are enough measurements to determine the angular width. For each case, normalized polarized radiances are simulated for the exact observation angles θ_v and φ_v, until the simulated peak width is consistent with the measured values.

The frequencies of retrieved maximum deviation angles are shown in Fig. 6 for square and Gaussian distributions of deviation angles, with respective average values of 1° and 1.8°. In more than 80% of the cases, the retrieved maximum deviation angle is less than 3°. It follows that, in most cases, the ice crystals are almost perfectly horizontally oriented, with slightly larger deviation angles more frequent for Gaussian distributions ($\simeq$40% of cases show $1° < \alpha_{\max} < 3°$, against $\simeq$15% for square distributions).

Following the previous case study (section 4c), once the maximum deviation angle is retrieved for a given case, polarized radiances are simulated for several aspect ratios A, estimating for each one the relative concentrations of horizontally oriented ice crystals n_h. These values are shown for square (Fig. 7a) and Gaussian (Fig. 7b) distributions of deviation angles, with average relative concentrations given in Table 2. The average frequency of horizontally oriented crystals in Table is between 6.2% and 21.4% if a square distribution is assumed, and between 5.4% and 8.6% if a Gaussian distribution is assumed. Moreover, for any aspect ratio the relative concentration of horizontally oriented crystals has more than a 60% probability of being under 10%. The second-highest frequency (Figs. 7a,b) is for a relative concentration of between 10% and 20%, but it is much lower (below 20%). The chosen angular distribution has only a small influence under these conditions.

5. Discussion and conclusions

The present study shows that, in the presence of horizontally oriented crystals within a cirrus cloud, their maximum deviation angle can be retrieved from spaceborne measurements of polarized radiances. This angle is generally very low, below 3° in most cases, with little

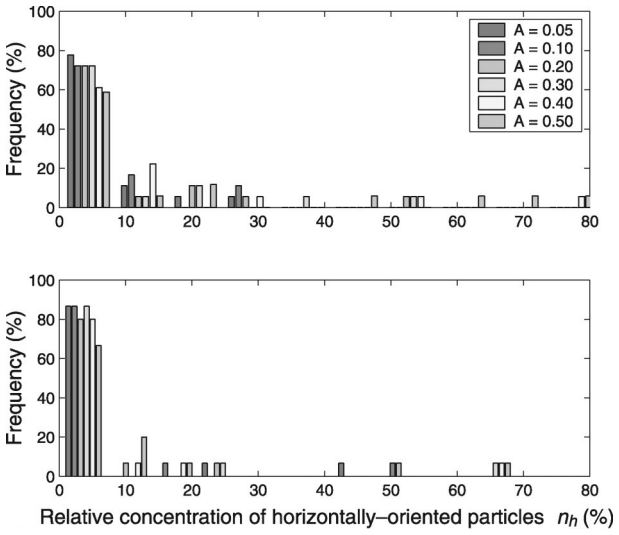

FIG. 7. Distribution of horizontally oriented crystals' concentrations n_h for (top) square distribution of crystal deviation and (bottom) Gaussian distribution of crystal deviation for different aspect ratios.

influence from the deviation angle distribution. Previous studies used other ground-based observations to retrieve this parameter: Sassen (1980), through a statistical analysis of direct photography, found oriented ice crystals in cirrus clouds were more likely to bear a Gaussian angular distribution, with a half-width angle below 1.4° for most particle shapes and a maximum value of 2.5°. Later, most studies took advantage of the rapid variation of the lidar signal near the zenith direction in the presence of oriented crystals: looking at the backscattered intensity, Platt et al. (1978) found a maximum deviation near 0.5°, while Thomas et al. (1990), by studying the more sensitive depolarization ratio, found a deviation angle no higher than 0.3°. However, these studies were mostly ground-based, and their conclusions are local. The present study draws consistent results from 31 cloud cases observed from satellite. Moreover, the concentration of oriented particles relative to the entire population of crystals, a parameter still unknown at this point, was found to be under 10% in most of the studied clouds. The application of this procedure to a high number of spaceborne measurements [from, e.g., POLDER-2 or Polarization and Anisotrophy of Reflectances for Atmospheric Sciences Coupled with Observations from a Lidar (PARASOL)] could give helpful insight into the orientation behavior of ice crystals in cirrus clouds, information that is otherwise very hard to get and still largely unknown.

However, there are still some limitations with this technique. For example, future progress in radiative transfer computations may show that the influence of multiple-scattering effects can not be considered similar in isotropic and anisotropic media, as was assumed in the present study (section 2b). Moreover, oriented ice crystals were taken as plates, which is the most likely hypothesis. However, oriented hollow columns can produce specific optical signatures similar to plate crystals (Sassen and Takano 2000), and in the future the way to discriminate these two shapes has to be investigated. Also, POLDER-1 measurements themselves have inherent limitations, the more important one being their spatial resolution of 6 km $\times$ 6 km. Even if still being able to obtain a signature of crystal orientation on such a large scale were to confirm the potential radiative implications of this phenomenon, there could be large variations in $\alpha_{\max}$ over an area so large. By analyzing smaller cloud areas through other techniques, the spatial variability of crystal orientations could be established on smaller scales, thereby assessing the representivity of POLDER-1 retrievals. Another problem occurs when the polarized radiances saturate the POLDER-1 sensors for some contiguous pixels. In such cases the retrieval is still possible, but the peak angular width is measured with a lower accuracy, which has an impact on the retrieved maximum deviation angle. Finally, the procedure shown in this paper only provides a range of correlated values: the relative concentrations and aspect ratios (section 4c). Although the variation of concentration with the supposed aspect ratio is quite small (less than 5%), any external retrieval of crystal shapes would significantly increase the reliability and credibility of the concentration results. When considering future observations from the PARASOL instrument, the collocated Cloud-Aerosol Lidar with Orthogonal Polarization (CALIOP) lidar from the National Aeronautics and Space Administration–Centre National d'Etudes Spatiales Cloud-Aerosol Lidar and Infrared Pathfinder Satellite Observaions (CALIPSO) mission (Winker and Wielicki 1999) could provide useful information about particle shape, thus constraining the retrieval.

Even with these limitations, valuable information can be gained about crystal orientation in cirrus clouds from spaceborne polarized radiometric measurements. Up to now, it remains the only known technique for retrieving this property on a global scale. As a next step to this study, the retrieval technique presented in this article could be applied to data from two new spaceborne instruments. First, the POLDER-2 instrument, located on *ADEOS-2*, which is already in orbit, has as of January 2003 begun to take measurements. Second, the PAR-

TABLE 2. Average concentrations of horizontally oriented crystals for different aspect ratios.

Aspect ratio A	0.05	0.1	0.2	0.3	0.4	0.5
Avg relative concentration n_h (square, %)	6.2	7.1	9.6	9.9	13.6	21.4
Avg relative concentration n_h (Gaussian, %)	5.4	6.0	6.7	7.2	8.0	8.6

ASOL mission, scheduled for launch in 2004, will provide another source of spaceborne POLDER measurements. Its location in a coordinated constellation of satellites (known as the ''A-Train'') will allow interaction with other spaceborne instruments, with potential improvements to the retrieval technique discussed in the present article. These results will greatly improve our understanding of the physical behavior of cirrus particles over the planet.

Acknowledgments. The results presented in this paper were obtained using data from CNES's POLDER instrument onboard NASDA's ADEOS platform. The authors are grateful to F.-M. Breon for processing the POLDER-1/Level-0 data.

REFERENCES

C.-Labonnote, L., G. Brogniez, M. Doutriaux-Boucher, and J.-C. Buriez, 2000: Modeling of light scattering in cirrus clouds with inhomogeneous hexagonal monocrystals. Comparison with in-situ and ADEOS-POLDER measurements. *Geophys. Res. Lett.*, **27,** 113–116.

——, ——, J. C. Buriez, M. Doutriaux-Boucher, J. F. Gayet, and A. Macke, 2001: Polarized light scattering by inhomogeneous hexagonal monocrystals: Validation with ADEOS-POLDER measurements. *J. Geophys. Res.*, **106,** 12 139–12 153.

Chepfer, H., G. Brogniez, P. Goloub, F. M. Breon, and P. H. Flamant, 1999: Observations of horizontally oriented ice crystals in cirrus clouds with POLDER-1/ADEOS-1. *J. Quant. Spectrosc. Radiat. Transfer,* **63,** 521–543.

——, P. Goloub, J. Riedi, J. D. Haan, J. W. Hovenier, and P. Flamant, 2001: Ice crystal shapes in cirrus clouds derived from POLDER/ADEOS-1. *J. Geophys. Res.*, **106,** 7955–7966.

——, P. Minnis, D. Young, L. Nguyen, and R. F. Arduini, 2002: Estimation of cirrus clouds effective ice crystals shapes using visible reflectances from dual-satellite measurements. *J. Geophys. Res.*, **107,** 4730, doi:10.1029/2000JD000240.

Deschamps, P. Y., F. M. Breon, M. Leroy, A. Podaire, A. Brickaud, J. C. Buriez, and G. Seze, 1994: The POLDER mission: Instrument characteristics and scientific objectives. *IEEE Trans. Geosci. Remote Sens.*, **32,** 598–615.

Goloub, P., J. L. Deuzac, M. Herman, and Y. Fouquart, 1994: Analysis of the POLDER polarization measurements performed over cloud covers. *IEEE Trans. Geosci. Remote Sens.*, **32,** 78–88.

——, N. Herman, H. Chepfer, P. Couvert, G. Brogniez, G. Seze, and J. Riedi, 2001: Cloud phase detection from POLDER/ADEOS. *J. Geophys. Res.*, **105,** 14 747–14 759.

Hagolle, O., and Coauthors, 1999: Results of POLDER in-flight calibration. *IEEE Trans. Geosci. Remote Sens.*, **37,** 1550–1566.

Hendry, A., and G. C. McCormick, 1976: Radar observations of the alignment of precipitation particles by electrostatic fields in thunderstorms. *J. Geophys. Res.*, **81,** 5353–5357.

Heymsfield, A. J., and C. M. R. Platt, 1984: A parameterization of the particle size spectrum of ice clouds in terms of the ambient temperature and the ice water content. *J. Atmos. Sci.*, **41,** 846–855.

Jayaweera, K., and B. J. Mason, 1965: The behavior of freely falling cylinders and cones in a viscous fluid. *J. Fluid Mech.*, **22,** 709.

Klett, J. D., 1995: Orientation model for particles in turbulence. *J. Atmos. Sci.*, **52,** 2276–2285.

Liou, K. N., and Y. Takano, 2002: Interpretation of cirrus cloud polarization measurements from radiative transfer theory. *Geophys. Res. Lett.*, **29,** 1313, doi:10.1029/2001GL014613.

List, R., and R. S. Schemenauer, 1971: Free-fall behavior of planar snow crystals, conical graupel and small hail. *J. Atmos. Sci.*, **28,** 110–115.

Lynch, D. K., S. D. Gedzelman, and A. B. Fraser, 1994: Subsuns, Bottlinger's rings, and elliptical halos. *Appl. Opt.,* **33,** 4580–4589.

Magono, C., 1953: On the growth of snow flakes and graupel. *Sci. Rep. Yokohama Natl. Univ., Ser. 1,* **2,** 18–40.

Masuda, K., H. Ishimoto, and T. Takashima, 2002: Retrieval of cirrus optical thickness and ice-shape information using total and polarized reflectance from satellite measurements. *J. Quant. Spectrosc. Radiat. Transfer,* **75,** 39–51.

Noel, V., H. Chepfer, G. Ledanois, and P. H. Flamant, 2001: Computation of a single-scattering matrix for nonspherical particles randomly or horizontally oriented in space. *Appl. Opt.,* **40,** 4365–4375.

——, G. Roy, L. Bissonnette, H. Chepfer, and P. H. Flamant, 2002: Analysis of lidar measurements at multiple incidence angles. *Geophys. Res. Lett.,* **29,** 1338, doi:10.1029/2002GL014828.

Ono, A., 1969: The shape and riming properties of ice crystals in natural clouds. *J. Atmos. Sci.,* **26,** 138–147.

Platt, C. M. R., N. L. Abshire, and G. T. McNice, 1978: Some microphysical properties of an ice cloud from lidar observations of horizontally oriented crystals. *J. Appl. Meteor.,* **17,** 1220–1224.

Podzimek, J., 1968: Aerodynamic conditions of ice crystal aggregation. *Proc. Int. Conf. on Cloud Physics*, Toronto, ON, Canada, Amer. Meteor. Soc., 295–299.

Riedi, J., M. Doutriaux-Boucher, P. Goloub, and P. Couvert, 2000: Global distribution of cloud top phase from POLDER/ADEOS I. *Geophys. Res. Lett.,* **27,** 1707–1710.

——, P. Goloub, and R. T. Marchand, 2001: Comparison of POLDER cloud phase retrievals to active remote sensors measurements at the ARM SGP site. *Geophys. Res. Lett.,* **28,** 2185–2188.

Sassen, K., 1980: Remote sensing of planar ice crystals fall attitude. *J. Meteor. Soc. Japan,* **58,** 422–433.

——, and Y. Takano, 2000: Parry arc: A polarization lidar, ray-tracing, and aircraft case study. *Appl. Opt.,* **39,** 6738–6475.

——, and S. Benson, 2001: A midlatitude cirrus cloud climatology from the Facility for Atmospheric Remote Sensing. Part II: Microphysical properties derived from lidar depolarization. *J. Atmos. Sci.,* **58,** 2103–2111.

——, K. N. Liou, Y. Takano, and V. I. Khvorostyanov, 2003: Diurnal effects in the composition of cirrus clouds. *Geophys. Res. Lett.,* **30,** 1539, doi:10.1029/2003GL017034.

Stephens, G. L., S.-C. Tsay, P. W. Stackhouse, and P. J. Flatau, 1990: The relevance of the microphysical and radiative properties of cirrus clouds to climate and climate feedback. *J. Atmos. Sci.,* **47,** 1742–1753.

Takano, Y., and K. N. Liou, 1989a: Solar radiative transfer in cirrus clouds. Part I: Single-scattering and optical properties of hexagonal ice crystals. *J. Atmos. Sci.,* **46,** 3–18.

——, and ——, 1989b: Solar radiative transfer in cirrus clouds. Part II: Theory and computation of multiple scattering in an anisotropic medium. *J. Atmos. Sci.,* **46,** 20–36.

Thomas, L., J. C. Cartwright, and D. P. Wareing, 1990: Lidar observations of the horizontal orientation of ice crystals in cirrus clouds. *Tellus,* **42B,** 211–216.

Trankle, E., and R. G. Greenler, 1987: Multiple-scattering effects in halo phenomena. *J. Opt. Soc. Amer.,* **4,** 591–599.

Van de Hulst, H. C., 1957: *Light Scattering by Small Particles.* Dover, 470 pp.

Winker, D., and B. Wielicki, 1999: The PICASSO-CENA mission. *Proc. SPIE,* **3870,** 26–36.

Wylie, D. P., W. P. Menzel, H. M. Woolf, and K. L. Strabala, 1994: Four years of global cirrus cloud statistics using HIRS. *J. Climate,* **7,** 1972–1986.